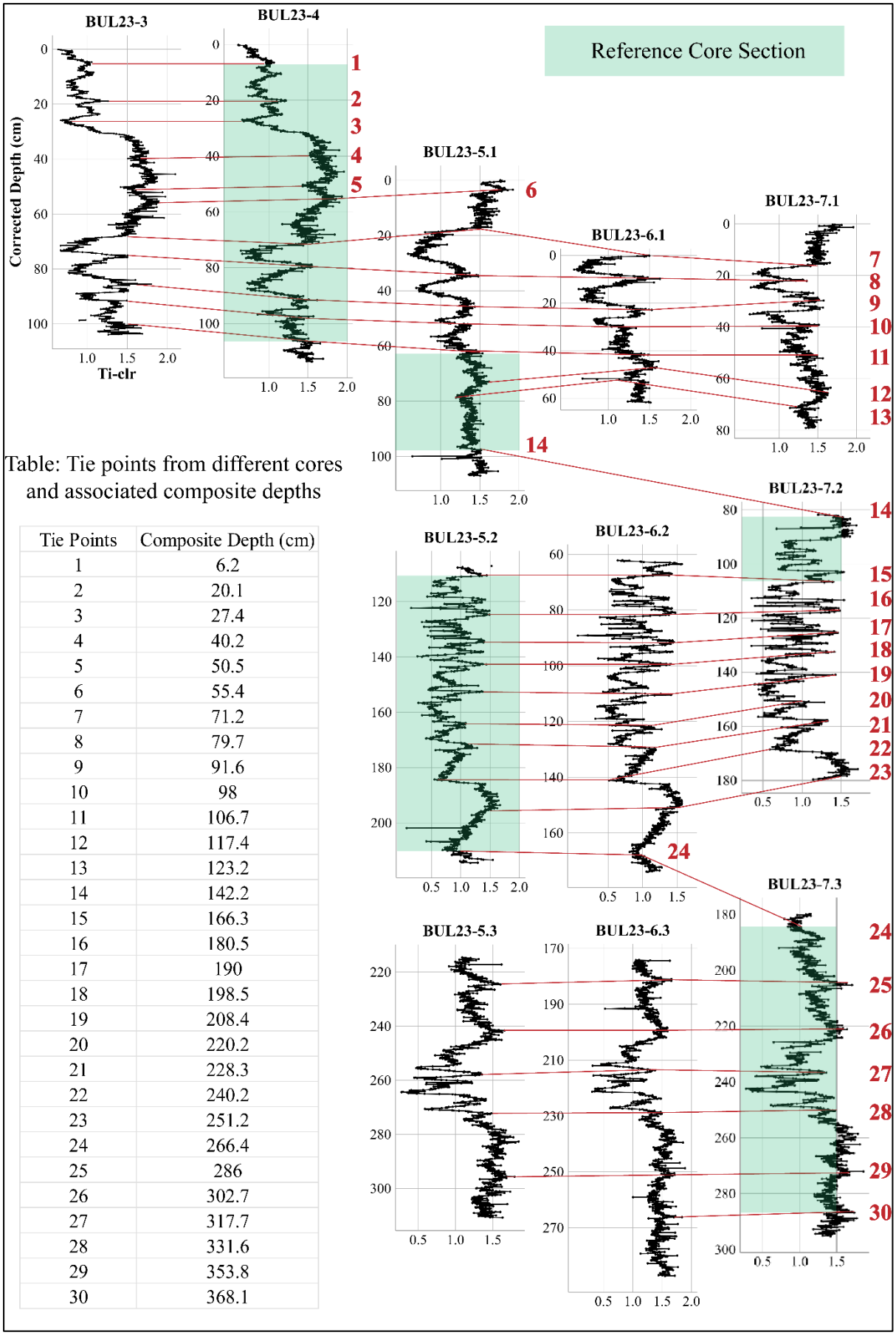


Table: Tie points from different cores and associated composite depths

Tie Points	Composite Depth (cm)
1	6.2
2	20.1
3	27.4
4	40.2
5	50.5
6	55.4
7	71.2
8	79.7
9	91.6
10	98
11	106.7
12	117.4
13	123.2
14	142.2
15	166.3
16	180.5
17	190
18	198.5
19	208.4
20	220.2
21	228.3
22	240.2
23	251.2
24	266.4
25	286
26	302.7
27	317.7
28	331.6
29	353.8
30	368.1

Figure S1. Core correlation, composite-depth construction and validation. Ti-clr profiles from UWITEC (BUL23-3 and BUL23-4) and piston (BUL23-5, BUL23-6, and BUL23-7) sediment cores from Lake Bullen Merri, plotted against core depth. Similar core sections were arranged adjacent to facilitate comparison, and corresponding Ti centred log-ratio (clr) peaks and troughs were matched to define 30 stratigraphic tie points. The green shading highlights the designated reference-core section. Composite depths were assigned to tie points relative to the reference core, and individual core-depth records were converted to composite depth by linear interpolation between tie points. Ca-clr data are provided as an independent validation of these correlations.

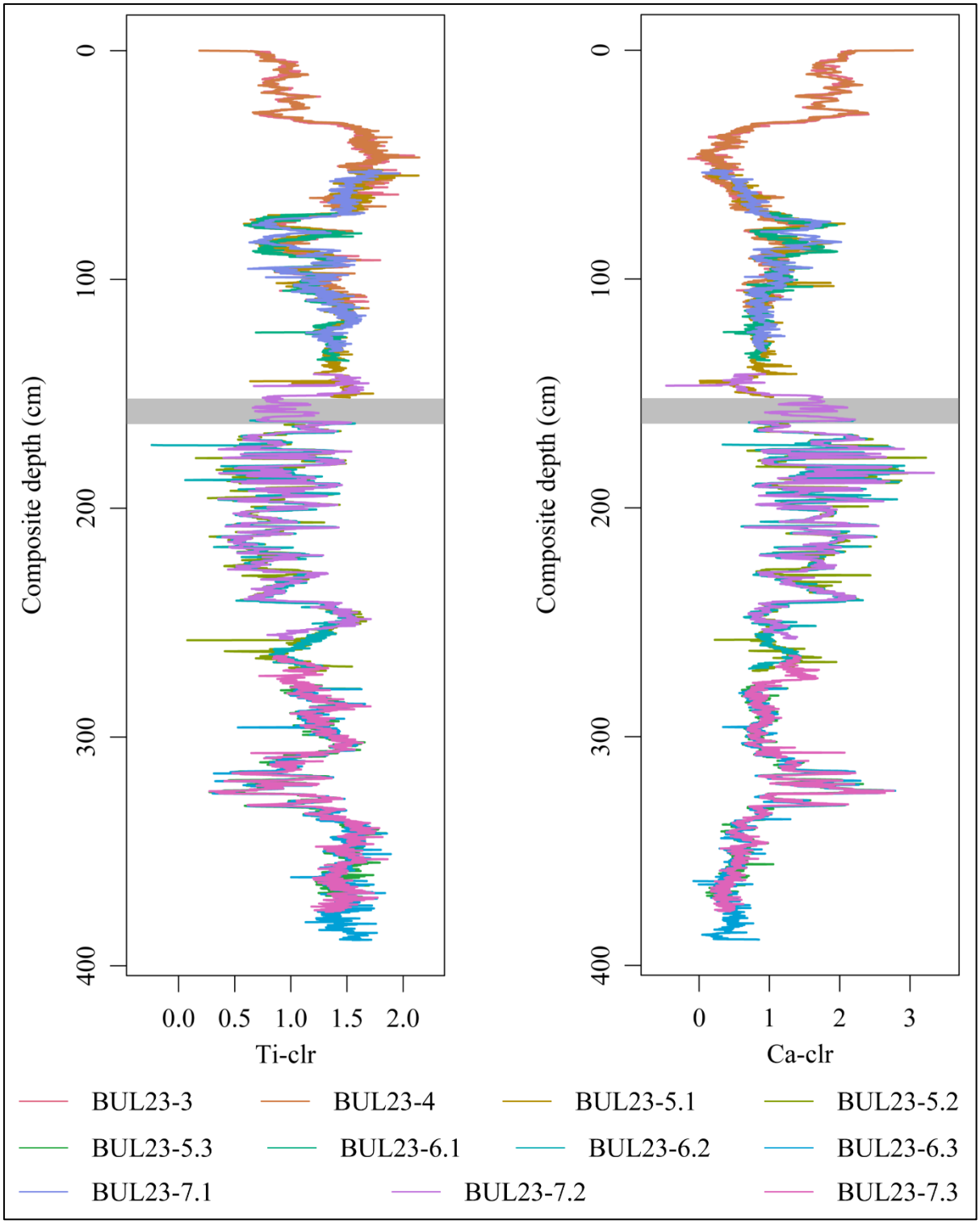


Figure S2. Validation of the Lake Bullen Merri composite depth scale. Ti-clr and independent Ca-clr records from UWITEC and piston sediment cores plotted against composite depth. Agreement among corresponding Ti-clr features, together with the alignment of independent Ca-clr variability, supports the stratigraphic correlations and composite-depth model. The grey band indicates the 152.1–163.2 cm composite-depth interval, for which samples could not be analysed, resulting in a data gap.

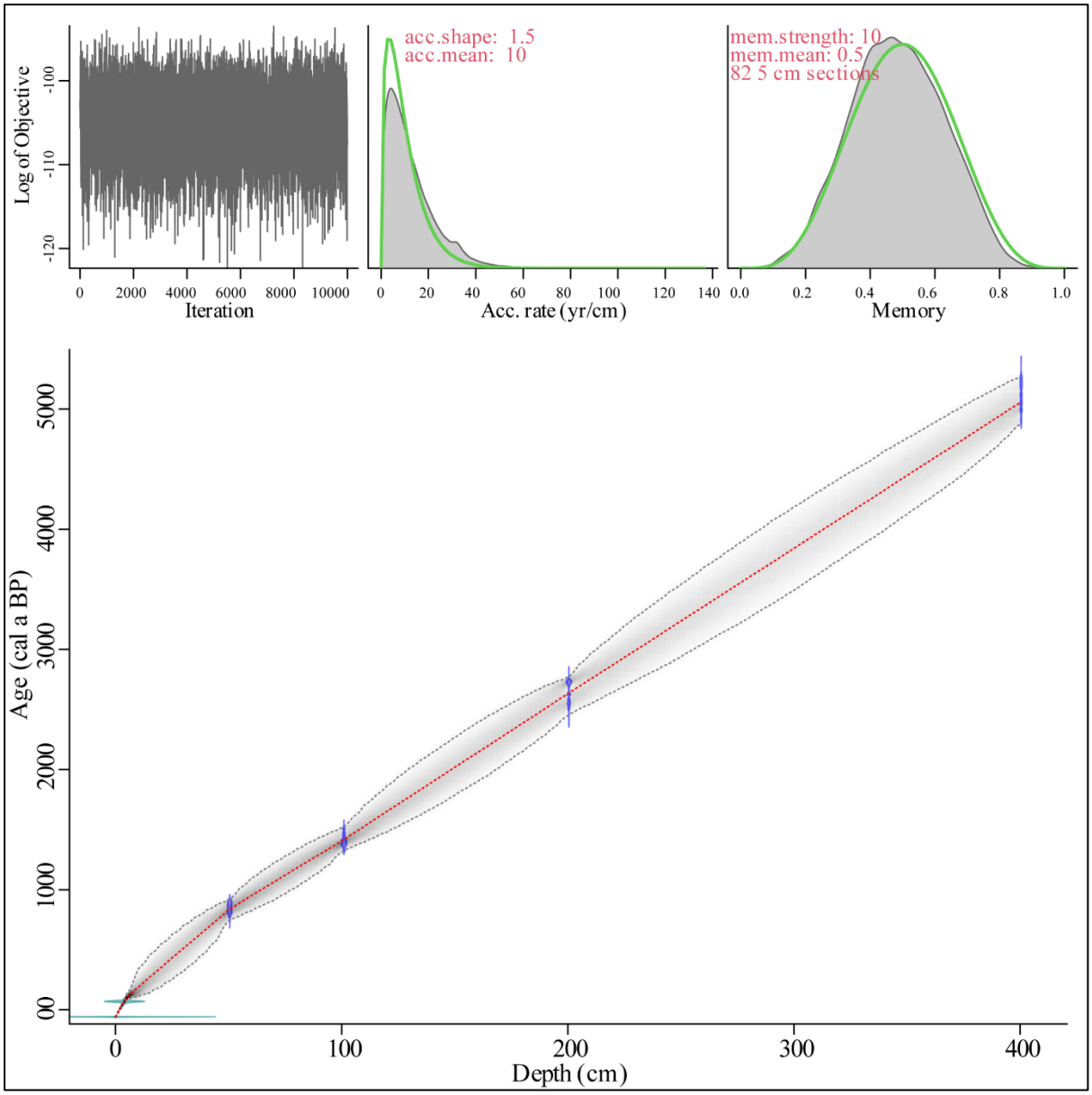


Figure S3. Bayesian age–depth model for the Tower Hill Main Lake core (Mills et al., 2013; Tyler et al., 2015). Blue markers show the probability distributions of radiocarbon-dated samples plotted against the left axis, while green markers indicate calendar ages assigned to the coring date and the first appearance of P. radiata. Grey dotted lines and shading represent the 95% confidence intervals, with darker shading indicating the most likely ages, and the red dotted line shows the weighted mean modelled age–depth curve

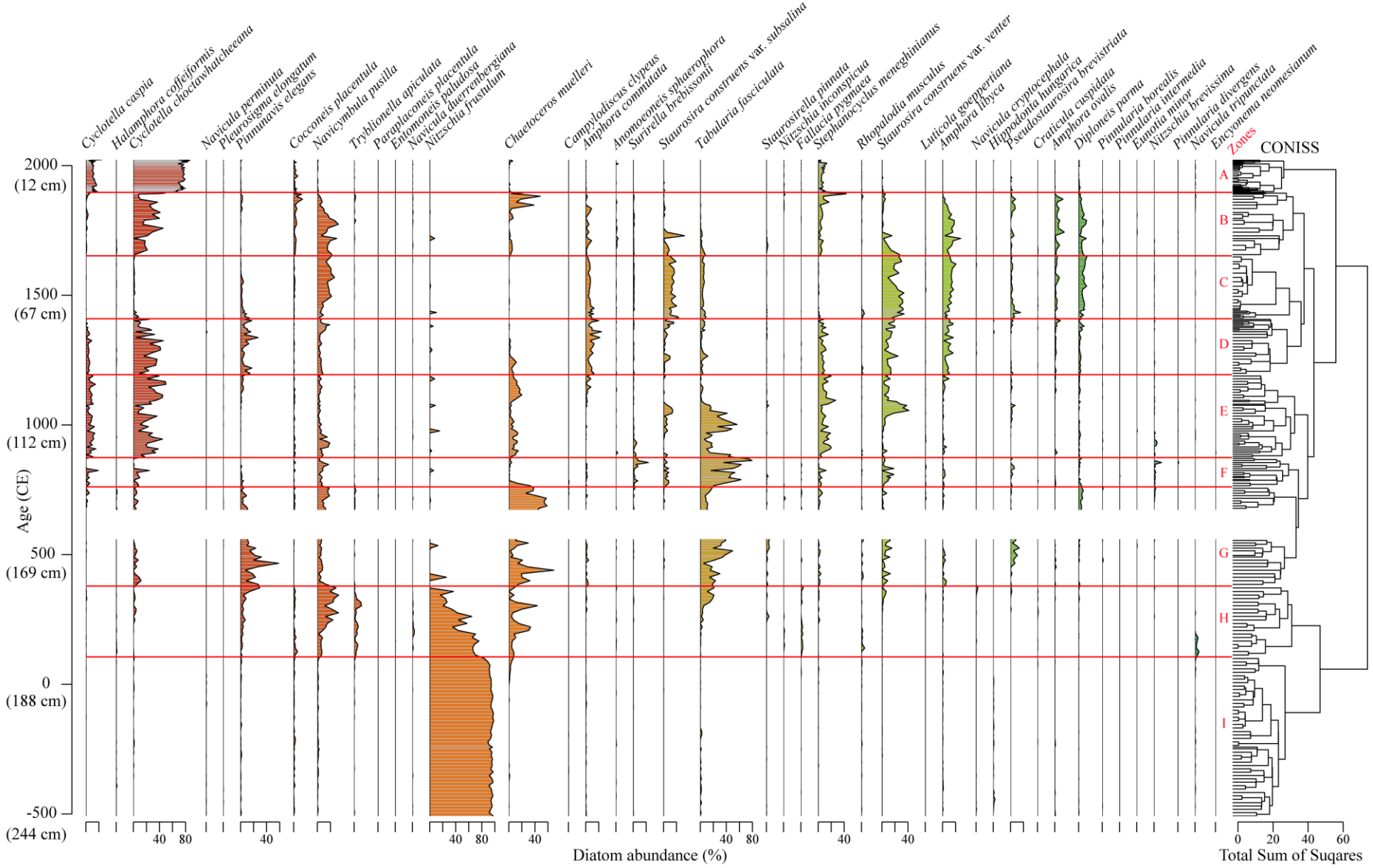

Cyclotella caspia
Halamphora coffeiformis
Cyclotella choctawhatcheeana
Navicula perminuta
Pleurosigma elongatum
Pinnunavis elegans
Cocconeis placentula
Navicymbula pusilla
Tryblionella apiculata
Paraplaconeis placentula
Entomoneis paludosa
Navicula duerrenbergiana
Nitzschia frustulum
Chaetoceros muelleri
Campylodiscus clypeus
Amphora commutata
Anomoeoneis sphaerophora
Surirella brebissonii
Staurosira construens var. subsalina
Tabularia fasciculata
Staurosirella pinnata
Nitzschia inconspicua
Fallacia pygmaea
Stephanocyclus meneghinianus
Rhopalodia musculus
Staurosira construens var. venter
Luticola goeppertiana
Amphora libyca
Navicula cryptocephala
Hippodonta hungarica
Pseudostaurosira brevistriata
Craticula cuspidata
Amphora ovalis
Diploneis parma
Pinnularia borealis
Pinnularia intermedia
Eunotia minor
Nitzschia brevissima
Pinnularia divergens
Navicula tripunctata
Encyonema neomesianum
Zones
CONISS
2000
(12 cm)
1500
(67 cm)
1000
(112 cm)
500
(169 cm)
0
(188 cm)
-500
(244 cm)
Age (CE)
A
B
C
D
E
F
G
H
I
40 80
40
40 80
40
40 80
40
40
0 20 40 60
Diatom abundance (%)
Total Sum of Suqares

Figure S4. Diatom stratigraphy for Lake Bullen Merri over the last 2500 years showing the relative abundances of all identified diatom species, with CONISS-derived assemblage zones (A–H) indicated to highlight major changes in community composition through time.

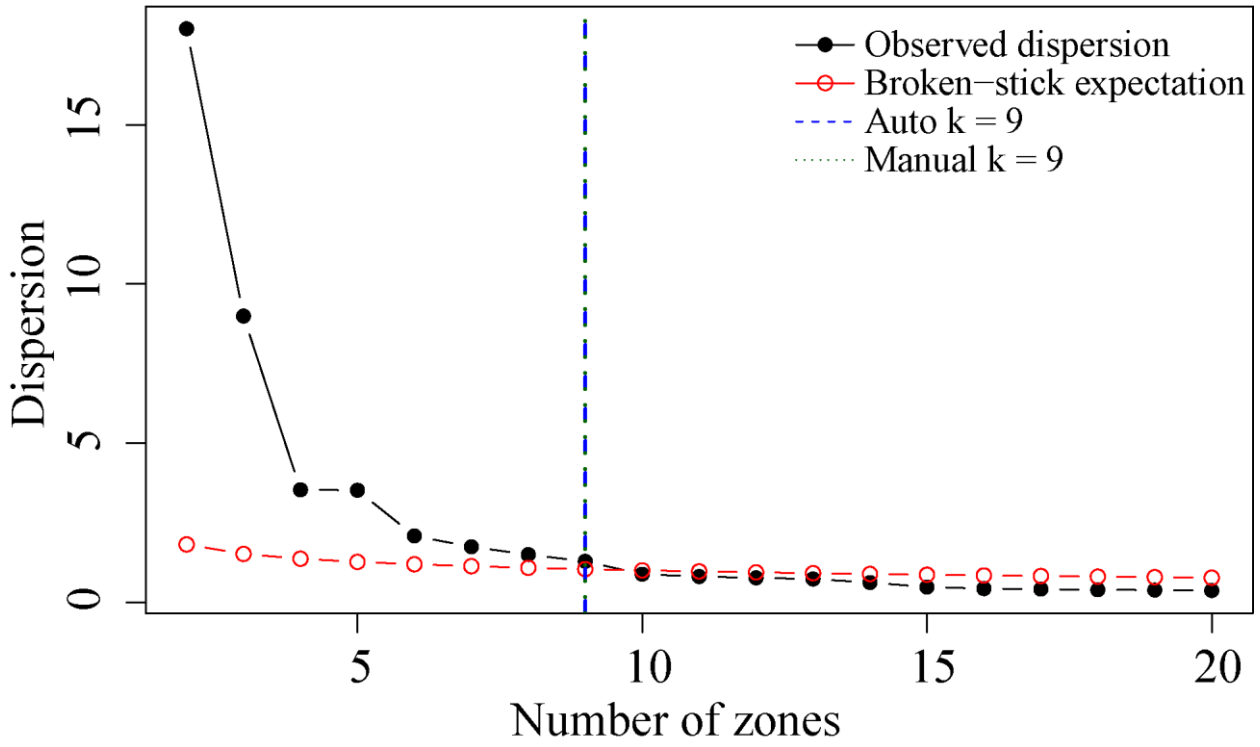


Figure S5. Broken Stick analysis used to determine the optimal number of significant diatom assemblage zones in the Lake Bullen Merri diatom record. The blue dashed line shows the automatically calculated Broken Stick model, while the black dotted line indicates the manually selected number and positions of zones, based on both the model output and visual inspection of the diatom stratigraphic data.

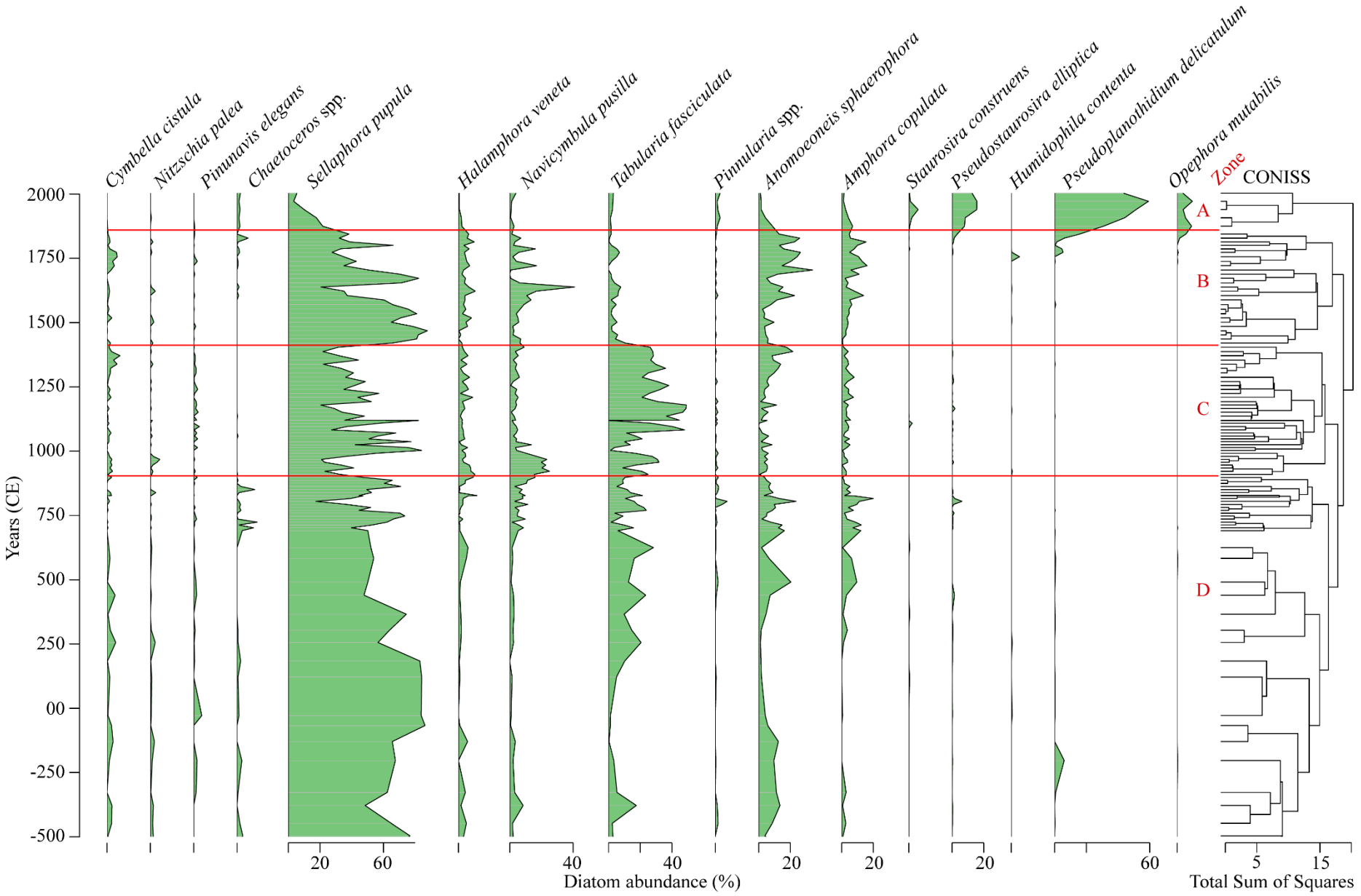

Cymbella cistula
Nitzschia palea
Pinunavis elegans
Chaetoceros spp.
Sellaphora pupula
Halamphora veneta
Navicymbula pusilla
Tabularia fasciculata
Pinnularia spp.
Anomoeoneis sphaerophora
Amphora copulata
Staurosira construens
Pseudostaurosira elliptica
Humidophila contenta
Pseudoplanothidium delicatulum
Opephora mutabilis
Zone
CONISS
A
B
C
D
Years (CE)
2000
1750
1500
1250
1000
750
500
250
00
-250
-500
20
60
40
40
20
20
20
60
5
15
Diatom abundance (%)
Total Sum of Squares

Figure S6. Diatom stratigraphy for Lake Tower Hill over the last 2500 years showing the relative abundances of all identified diatom species, with CONISS-derived assemblage zones (A–D) indicated to highlight major changes in community composition through time (Mills et al., 2013; Tyler et al., 2015).

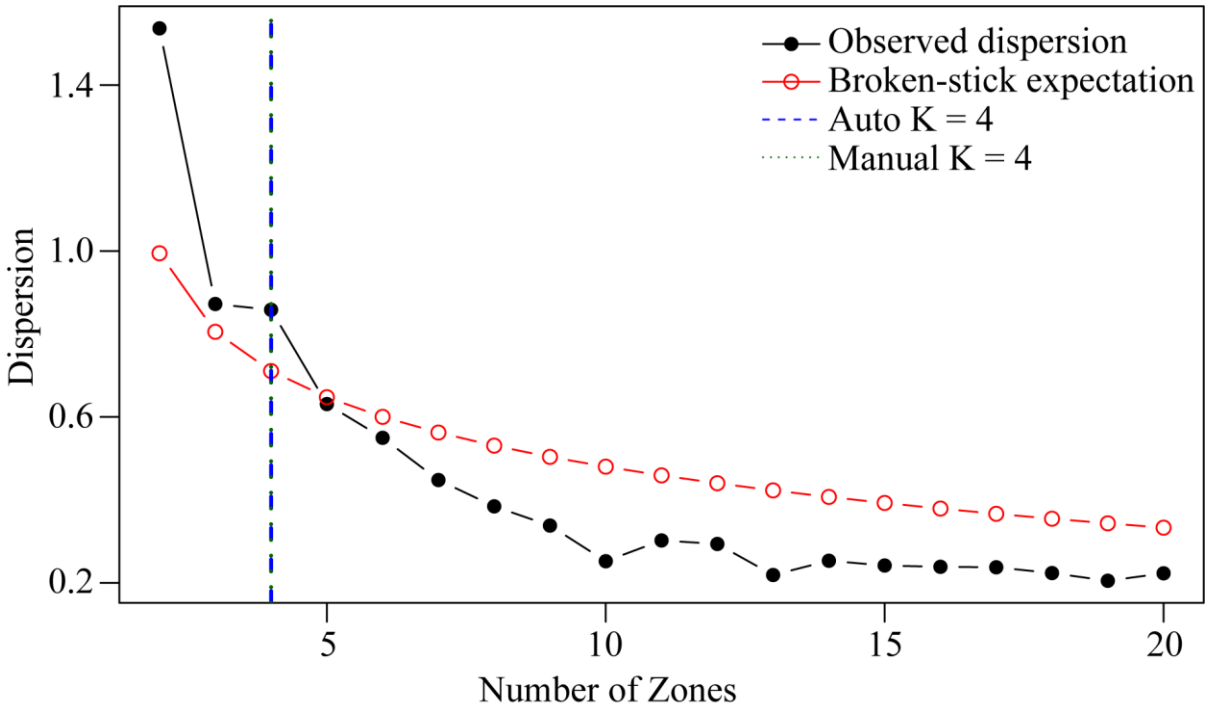


Figure S7. Broken Stick analysis used to determine the optimal number of significant diatom assemblage zones in the Lake Tower Hill diatom record. The blue dashed line shows the automatically calculated Broken Stick model, while the black dotted line indicates the manually selected number and positions of zones, based on both the model output and visual inspection of the diatom stratigraphic data.

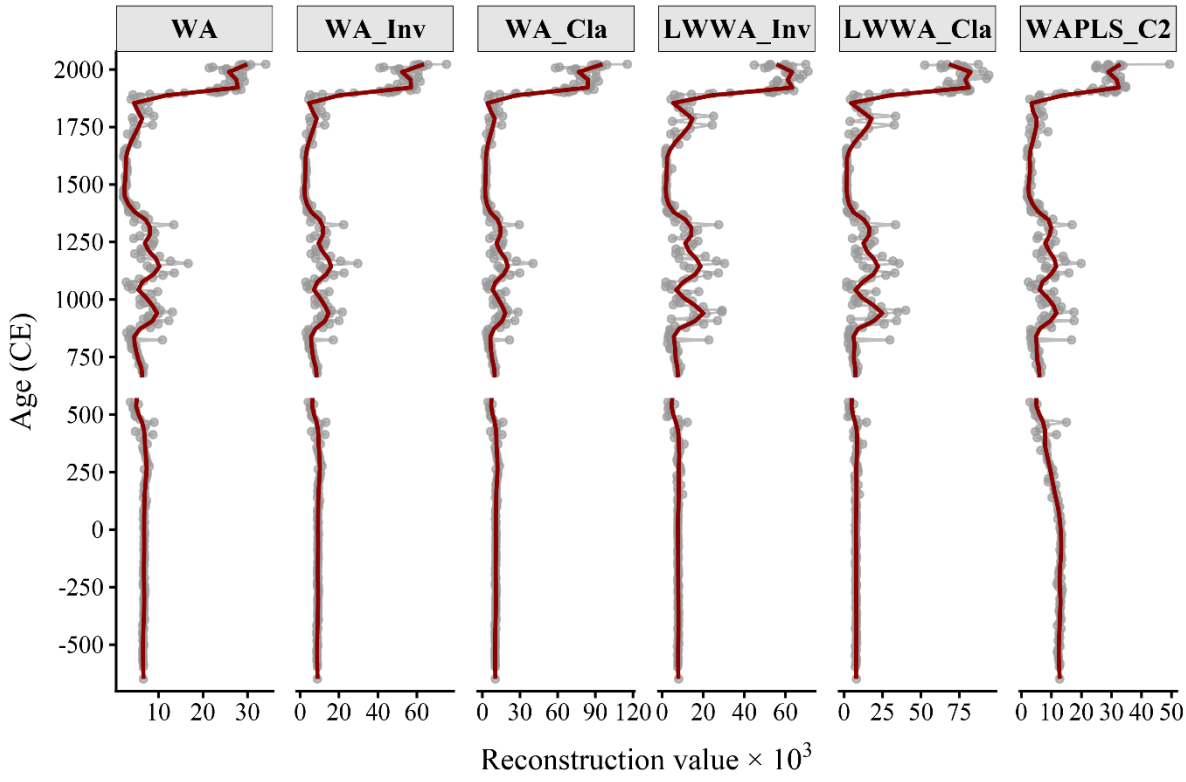


Figure S8. EC reconstructions for Lake Bullen Merri over the last 2500 years using different diatom–EC calibration methods (WA, WA-Inv, WA-Cla, LWWA-Inv, LWWA-Cla and WA-PLS) (Rahman et al., 2026). All methods show nearly identical temporal trends, indicating robust patterns of salinity change across the record. Red lines indicate a locally weighted sum of squares (loess) fit with span = 0.1 (Cleveland et al., 2017).

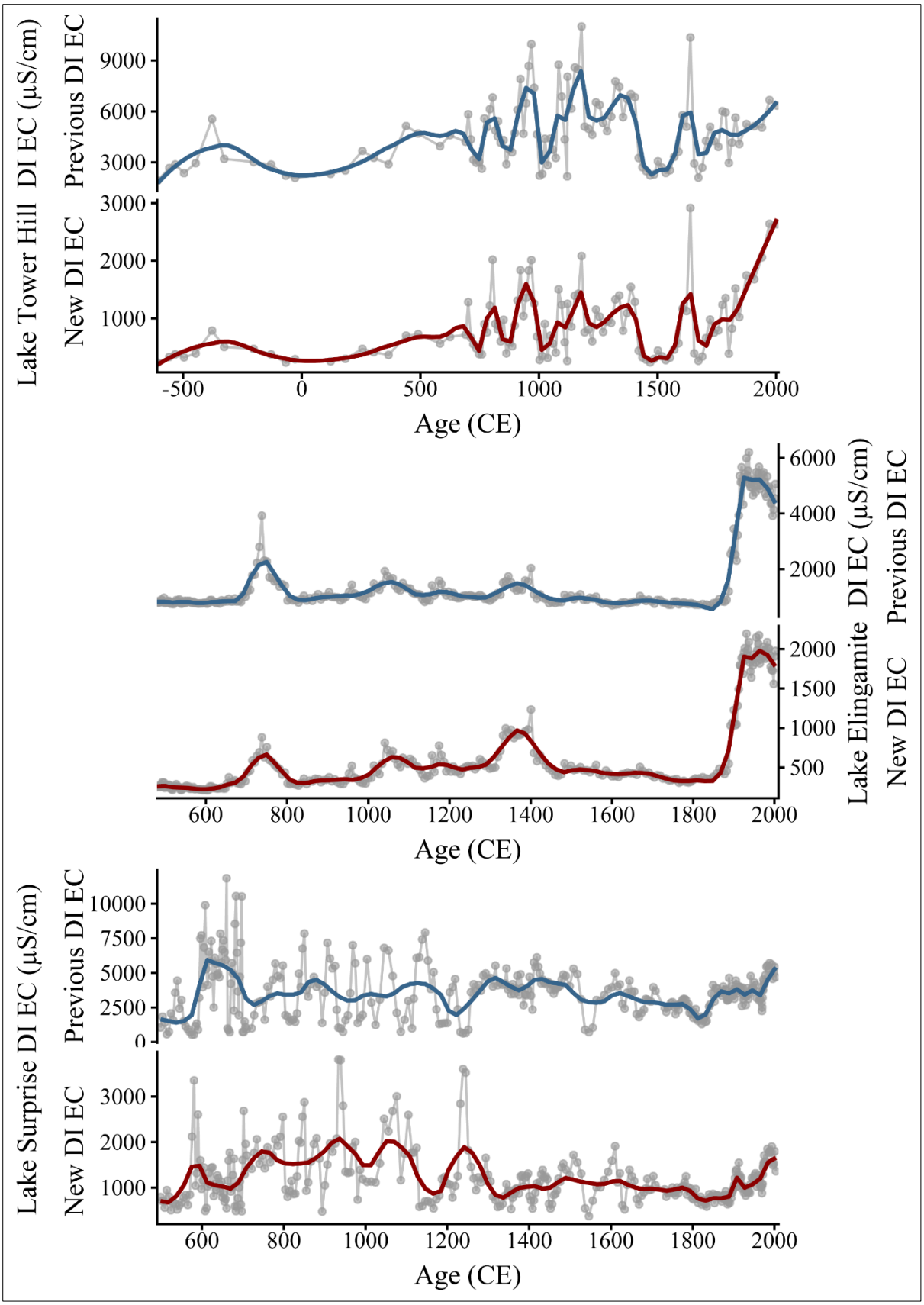


Figure S9. Reconstructed Lake-water conductivity (EC) for Tower Hill Main Lake (Mills et al., 2013), Lake Elingamite and Lake Surprise (Barr et al., 2014), showing both the original reconstructions and

those obtained using the updated diatom–EC transfer function of Rahman et al. (2026). The new reconstructions yield more realistic absolute EC estimates and improved analogue performance compared with the original versions. Red lines indicate locally weighted scatterplot smoothing (loess) fits with span = 0.1 (Cleveland et al. 2017).

a.
b.
c.
d.
e.
f.
g.
h.
i.
j.
Lake Bullen Merri
DI EC (µS/cm)
5000
10000
15000
Lake Tower Hill
DI EC (µS/cm)
1000
2000
3000
Lake Elingamite
DI EC (µS/cm)
250
500
750
1000
1250
Lake Surprise
DI EC (µS/cm)
1000
2000
3000
Lake Keilambete
Water Depth (m)
25
20
15
10
Snowy Flat
Water Table Depth (cm)
5
10
15
20
Rebecca Lagoon
PI Precipitation (mm)
300
200
100
0
Kubla Khan Cave
Speleothem Mg (ppm)
1000
2000
3000
4000
Coorong Lagoon
Bivalve δ18O (‰)
3.0
3.5
4.0
4.5
5.0
Lashmars Lagoon
Ostracod δ18O (‰)
2
4
6
8
-500
-250
0
250
500
750
1000
1250
1500
1750
2000
Age (CE)

Figure S10. Comparison of reconstructed hydroclimate variability from a. Lake Bullen Merri with three nearby diatom-based EC records from b. Lake Tower Hill (Mills et al., 2013), c. Lake Elingamite, and d. Lake Surprise (c–d; Barr et al., 2014), e. Lake Keilambete (Wilkins et al., 2013), f. Snowy Flat (Zheng et al., 2025), g. Rebecca Lagoon (Saunders et al., 2012), h. Kubla Khan Cave (Cooley et al., 2026), i. Coorong Lagoon (Chamberlayne et al., 2023), J. Lashmars Lagoon (Rahman et al., 2025). Yellow panel marks the interval interpreted as strongly influenced by direct anthropogenic impact. Black lines indicate a locally weighted sum of squares (loess) fit with span = 0.1 (Cleveland et al., 2017).

References:

Barr, C., Tibby, J., Gell, P., Tyler, J., Zawadzki, A., and Jacobsen, G. E.: Climate variability in south-eastern Australia over the last 1500 years inferred from the high-resolution diatom records of two crater lakes, Quat. Sci. Rev., 95, 115–131, 2014.

Chamberlayne, B. K., Tyler, J. J., Haynes, D., Shao, Y., Tibby, J., and Gillanders, B. M.: Hydrological change in southern Australia over 1750 years: a bivalve oxygen isotope record from the Coorong Lagoon, Clim. Past, 19, 1383–1396, 2023.

Cleveland, W. S., Grosse, E., and Shyu, W. M.: Local regression models, in: Statistical models in S, Routledge, 309–376, 2017.

Cooley, S. R., Fletcher, M.-S., Drysdale, R. N., MacGregor, C., Treble, P. C., Hua, Q., Hellstrom, J., Demény, A., Greig, A., and Eberhard, R.: Holocene hydroclimate, fire, and the persistence of coniferous sub-alpine rainforest in Tasmania, Australia, Quat. Sci. Rev., 384, 109996, https://doi.org/https://doi.org/10.1016/j.quascirev.2026.109996, 2026.

Mills, K., Gell, P. A., and Kershaw, A. P.: The Recent Victorian Drought and its Impact: Without Precedent?, Rural Industries Research and Development Corporation, 2013.

Rahman, M., Duxbury, L., Cadd, H., Klaebe, R., Jacobsen, G., Tibby, J., and Tyler, J.: A 2000-year record of hydroclimate variability inferred from oxygen isotopes in lake sediments on Kangaroo Island (Karti/Karta), South Australia, Quat. Sci. Rev., 363, 109443, 2025.

Rahman, M., Tyler, J., Barr, C., Reid, M., Gell, P., and Tibby, J.: Development of a diatom-electrical conductivity transfer function for temperate Australian lakes, Manuscript submitted to Hydrobiologia (HYDR-S-26-01541), 2026.

Saunders, K. M., Kamenik, C., Hodgson, D. A., Hunziker, S., Siffert, L., Fischer, D., Fujak, M., Gibson, J. A. E., and Grosjean, M.: Late Holocene changes in precipitation in northwest Tasmania and their potential links to shifts in the Southern Hemisphere westerly winds, Glob. Planet. Change, 92, 82–91,

2012.

Tyler, J. J., Mills, K., Barr, C., Sniderman, J. M. K., Gell, P. A., and Karoly, D. J.: Identifying coherent patterns of environmental change between multiple, multivariate records: an application to four 1000-year diatom records from Victoria, Australia, Quat. Sci. Rev., 119, 94–105, 2015.

Wilkins, D., Gouramanis, C., De Deckker, P., Fifield, L. K., and Olley, J.: Holocene lake-level fluctuations in Lakes Keilambete and Gnotuk, southwestern Victoria, Australia, The Holocene, 23, 784–795, 2013.

Zheng, X., Hope, G., and Mooney, S. D.: The reconstruction of water table depth over the past 3100 years in south-eastern Australia using testate amoebae and potential implications for Pacific climatic variability, Palaeogeogr. Palaeoclimatol. Palaeoecol., 679, 113264, https://doi.org/https://doi.org/10.1016/j.palaeo.2025.113264, 2025.